Chemical Research in Toxicology

pubs.acs.org/crt

Article

Binding of *N*-(1,3-Dimethylbutyl)-*N*′-phenyl-*p*-phenylenediamine Quinone (6PPDQ) to Mitochondrial Proteins Provokes Mitochondria Dysfunction

Naijie Wei, Xiaowen Yan,* Mingyue Yu, Rong Li, Zhixin Xiao, Shi Chen, Limin Yang, Qiuquan Wang,* Qian Liu, and Guibin Jiang

Cite This: *Chem. Res. Toxicol.* 2026, 39, 283−292

Read Online

ACCESS | Metrics & More | Article Recommendations | Supporting Information

ABSTRACT: *N*-(1,3-Dimethylbutyl)-*N*′-phenyl-*p*-phenylenediamine Quinone (6PPDQ) not only causes acute mortality in salmon but also induces toxicities in other living organisms. The electrophilic quinone moiety in the 6PPDQ molecular structure can participate in binding to the cysteine residues that ubiquitously exist in protein nucleophiles, which are responsible for its toxicities. Out of the 82 6PPDQ-bonded proteins found in the human model cell line A549 on the sulfhydryl-reactive proteomics platform, which enables the precise identification of covalent binding protein targets of a pollutant, we discovered three 6PPDQ-bonded mitochondrial proteins—NDUS6, COX5B, and ATP5PB—that are involved in mitochondrial dysfunction for the first time. They impede the function of mitochondria, as witnessed by the decreased enzymatic activities of mitochondrial respiratory chain Complexes I (27.63%) and IV (23.11%), the decreased cellular ATP content (19.94%), and the reduced mitochondrial membrane potential (3.2-fold), as well as the elevated mitochondrial ROS level (2.2-fold) under the environmentally relevant 8.9 μg/L 6PPDQ exposure compared to the controls. Our findings provide experimental evidence for elucidating 6PPDQ's toxicities at the molecular level, and the knowledge learned will enhance the public's awareness of the adverse impacts of environmental pollution on health.

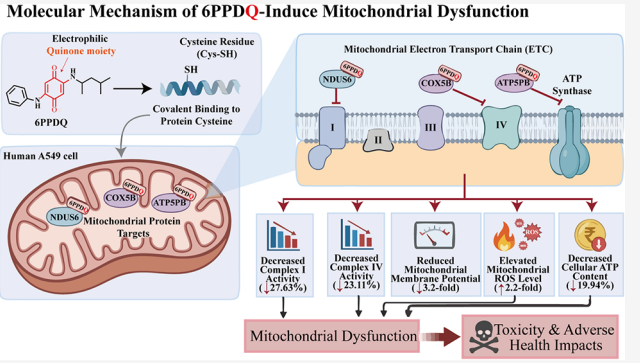

Downloaded via XIAMEN UNIV on April 22, 2026 at 00:33:19 (UTC).
See https://pubs.acs.org/sharingguidelines for options on how to legitimately share published articles.

INTRODUCTION

N-(1,3-Dimethylbutyl)-*N*′-phenyl-*p*-phenylenediamine quinone (6PPDQ) generally comes from the oxidation of its parent compound, *N*-(1,3-dimethylbutyl)-*N*′-phenyl-*p*-phenylenediamine (6PPD), an antioxidant additive in the rubber industry, by ozone in the environment and P450 enzymes in living organisms.[1,2] Recent studies have documented that, not limited to salmonids, 6PPDQ has also been reported to cause poisoning symptoms in cross-species organisms.[3] As an emerging contaminant, 6PPDQ was determined in various environmental samples, such as runoff water (86−19,000 ng/L) and surface water (0.38−2300 ng/L); air particles $PM_{2.5}$ (2.44−7250 pg/m^3) and PM_{10} (0.16−39.2 pg/m^3); E-waste dust (87.1−2850 ng/g), road dust (4.02−2369 ng/g), and house dust (0.62−106 ng/g); urban river sediments (1.87−18.2 ng/g); and roadside soils (9.50−936 ng/g).[3,4] More seriously, 6PPDQ has also been found in human samples. For example, 6PPDQ in the urine samples of pregnant women, nonpregnant adults, and children was determined to be 2.91 ng/mL, 0.40 ng/mL, and 0.076 ng/mL;[5] and the average concentration of 6PPDQ in the cerebrospinal fluid of Parkinson's Disease patients was 11.18 ng/mL,[6] as well as 6PPDQ in human plasma reached up to 1.81 ng/mL.[7−9] This widespread presence of 6PPDQ raises concerns regarding its potential health impacts on human beings.[10] Having a close look at the molecular structures of 6PPDQ and 6PPD, the key difference between them is the quinone moiety in 6PPDQ and the phenyl in 6PPD (Scheme 1A). The stronger electrophilicity of the quinone moiety in 6PPDQ should be the molecular basis that leads to its much more significant tendency to attack the nucleophilic groups of effector proteins, which initially triggers its toxic processes.

In order to understand the toxicity of 6PPDQ, we started with studies of 6PPDQ's reactivity toward typical nucleophilic amino acid residues existing in a peptide and/or a protein, confirming its superior chemical binding ability to the cysteine residue. Moreover, 6PPDQ is prone to being adsorbed and enriched onto atmospheric particulates because of its high

Received: June 17, 2025
Revised: February 3, 2026
Accepted: February 11, 2026
Published: February 19, 2026

ACS Publications

© 2026 American Chemical Society

Scheme 1. (A) The Transformation of 6PPD into 6PPDQ. (B) Desthiobiotin Iodoacetamide (DBIA)-Mediated Sulfhydryl-Reactive Proteomics Platform. (C) Sulfhydryl-Reactive Proteins and 6PPDQ-Bonded Proteins, Bioinformatic Analysis, and Three 6PPDQ-Bonded Mitochondrial Proteins: NDUS6, COX5B, and ATP5PB

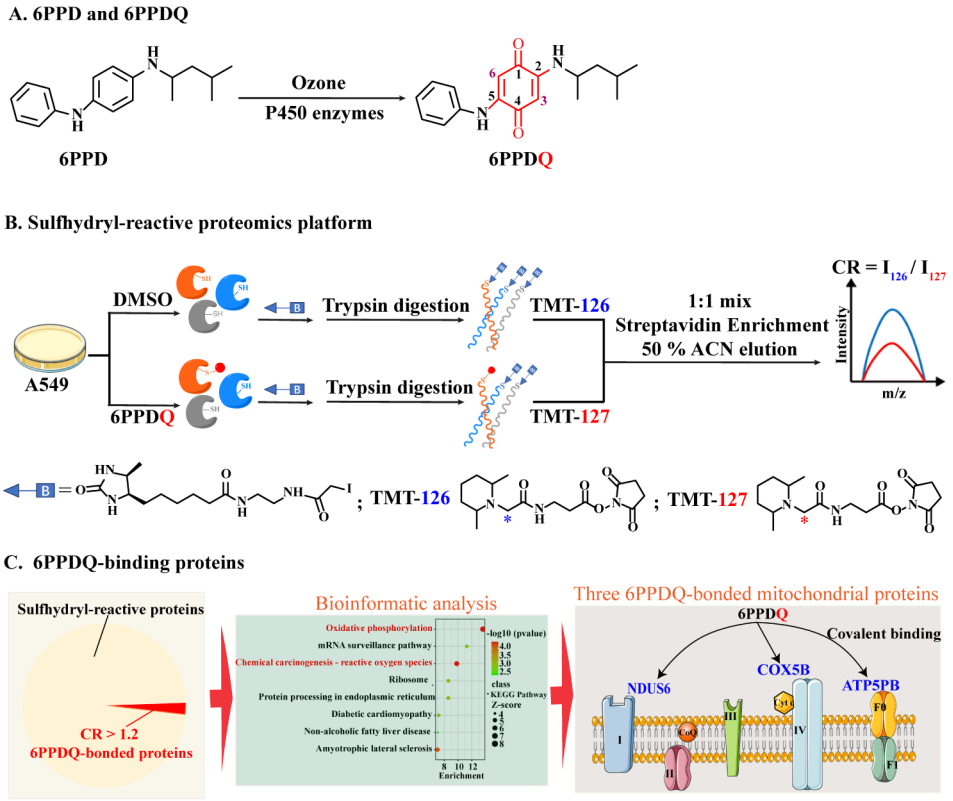

Competition ratio (CR) = Intensity of 126 mass reporter / Intensity of 127 mass reporter

LogK_{OA} value (12.46),[11] resulting in a higher human lung exposure risk through breathing. Therefore, we chose human nonsmall cell lung cancer cells (A549) to inspect 6PPDQ-binding proteins on the desthiobiotin iodoacetamide (DBIA)-mediated sulfhydryl-reactive proteomics platform (Scheme 1B) established here, and their resided biological pathways and functions were annotated via bioinformatics (Scheme 1C). Among the 82 6PPDQ-bonded proteins found, three 6PPDQ-bonded mitochondrial proteins—NADH dehydrogenase [ubiquinone] iron−sulfur protein 6 (NDUS6), Cytochrome c oxidase subunit 5B (COX5B), and ATP synthase F(0) complex subunit B1 (ATP5PB)—located on the pervasive mitochondrial oxidative phosphorylation pathway, were discovered to be responsible for mitochondrial dysfunction (Scheme 1C). The mitochondrial dysfunction caused by the binding of 6PPDQ to these three conserved mitochondrial proteins was evidenced by the fact that they decrease the enzyme activities of Complex I and IV, the mitochondrial membrane potential ($\Delta\psi m$), and ATP content, as well as elevate ROS generation. These findings open a window to understand the possible molecular mechanism of 6PPDQ's toxicity. We hope that our approach not only sets an example for the toxicological examination of other environmental pollutants at the molecular level but also will benefit the discovery of the key proteins and/or mechanisms behind the acute and specific lethal toxicity of 6PPDQ to salmonids in the future.

MATERIALS & METHODS

Characterization of 6PPDQ Reactivity toward Nucleophiles

6PPDQ (0.03 μM and/or 0.3 μM, the maximum soluble concentration in 0.5% DMSO) (see Text S1 for details of the 6PPDQ synthesis procedure) was incubated individually with nucleophilic amino acids (Aladdin, Bio-Ultra, ≥99%, China), *N*-acetylcysteine (NAC, Aladdin, Bio-Ultra, ≥99%, China), and reduced glutathione (GSH, Aladdin, Bio-Ultra, ≥99%, China) of 10 mM each in phosphate-buffered saline (PBS, pH = 7.2, Sigma-Aldrich, U.S.A.). After incubation at 37 °C for 24 h, the reaction products were analyzed by using high-performance liquid chromatography-electrospray ionization Q-TOF mass spectrometry (HPLC-ESI-Q-TOF-MS). The reaction products (100 μL) were first separated on an HPLC-20AD (Shimadzu, Japan) with an Inertsil ODS-3 C18 column (5 μm, 4.6 mm I.D. × 150 mm in length, Shimadzu) online coupled to Bruker Impact II ESI-Q-TOF-MS for mass analysis. Mobile phases A (0.1% formic acid in water) and B (0.1% formic acid in acetonitrile) were used for gradient elution. The gradient chromatographic elution program was as follows: 0−5 min, 98% A; 5−22 min, 98∼10% A; and 22−27 min, 5% A at a flow rate of 1 mL/min. ESI-Q-TOF-MS: ion polarity, positive; end plate offset, 500 V; capillary voltage, 4500 V; nebulizer, 0.4 bar; dry gas, 4 L/min; N_2 dry temperature, 180 °C; mass range, 150−1300 m/z; scan mode, MS; spectra rate, 3 Hz; quadrupole, ion energy, 4.0 eV; collision cell, collision energy, 7.0 eV; transfer time, 100.0 μs; detector voltage, 2360 V. Human serum albumin (HSA, 25 μM) (Sigma-Aldrich, ≥99% agarose gel electrophoresis, U.S.A.) was first denatured in 8 M

https://doi.org/10.1021/acs.chemrestox.5c00250
Chem. Res. Toxicol. 2026, 39, 283−292

urea and reduced with 2 mM Tris(2-carboxyethyl)phosphine hydrochloride (TCEP, Sigma-Aldrich, Bio-Ultra, ≥98% NMR, U.S.A.) at 37 °C for 1 h, followed by reaction with 6PPDQ (0.3 μM) for 4 h. The reaction was then quenched by alkylation with 5 mM iodoacetamide (Sigma-Aldrich, ≥99% NMR, crystalline, U.S.A.) and incubated at room temperature in the dark for 30 min. After diluting the urea concentration to 2 M, trypsin (Promega, Trypsin Gold, Mass Spectrometry grade, Germany) was added (enzyme:substrate mass ratio = 1:25) and incubated at 37 °C for 17 h for digestion. Finally, HPLC-ESI-Q-TOF-MS/MS was performed to analyze 6PPDQ modification on HSA. Detailed HPLC-ESI-MS/MS conditions are provided in Text S2.

Cell Culture and Cell Lysis

The A549 cells (ATCC) were cultured in DMEM (Sangon Biotech, China) containing 10% heat-inactivated fetal bovine serum (Sangon Biotech, China) and 100 units/mL penicillin−streptomycin (BioInd, Israel) in a humidified 37 °C incubator with 5% CO_2. Until ∼80% confluent, the cells were harvested using 0.05% trypsin (Sigma-Aldrich, U.S.A.), they were then pelleted by centrifugation (300 *g*, 4 min at 4 °C) and washed once with PBS. Afterward, the cell pellets were immediately lysed using a 1% Triton-100 lysis buffer (Beyotime, China) supplemented with 1 mM phenylmethanesulfonyl fluoride (PMSF, Beyotime, China) at 4 °C for 15 min and centrifuged at 12,000 *g* for 10 min at 4 °C. The supernatant was carefully collected as the cell lysate for further use.

DBIA-Mediated Sulfhydryl-Reactive Proteomics Platform

Sulfhydryl-reactive proteomics analysis was conducted based on the reported method[12] with some modifications (detailed procedures are provided in the Supporting Information). Cell lysates (100 μg each) from DMSO-treated (the control) and 0.3 μM 6PPDQ-exposure groups were individually incubated with 500 μM desthiobiotin iodoacetamide (DBIA) probe (MedChemExpress, China) at room temperature in the dark for 1 h for the reaction between iodoacetamide in DBIA and cysteine residues in the proteins. Subsequently, 10 mM dithiothreitol (DTT, Thermo Fisher, U.S.A.) was added for reduction at 37 °C for 1 h, followed by alkylation with 40 mM iodoacetamide at room temperature in the dark for 30 min. The proteins were precipitated using a methanol/chloroform/H_2O (4/1/3) mixture. After centrifugation at 14,000 *g* at 4 °C for 10 min, the supernatant containing unreacted DBIA was discarded. The protein precipitate was resuspended in 100 mM triethylammonium bicarbonate buffer (TEAB, Thermo Fisher, U.S.A.) and digested with trypsin at 37 °C for 17 h. The digested peptides in the control and 6PPDQ-exposure groups were labeled, respectively, by the isotopically tandem mass tags TMT-126 and TMT-127 according to the TMTduplex labeling kit protocol (Thermo Fisher) through amidation reactions between the *N*-hydroxysuccinimide in TMTs and the *N*-terminal α-amino group and/or lysine side-chain ε-amino group of the trypsin-digested peptides,[13] and then equal amounts of labeled peptides from both groups were combined into a pooled sample. DBIA-labeled peptides were enriched using streptavidin magnetic beads (Thermo Fisher, U.S.A.). The enriched peptides were eluted from the streptavidin magnetic beads using 50% acetonitrile containing 0.1% trifluoroacetic acid and finally subjected to HPLC-ESI-Orbitrap-MS/MS for quantitative analysis. Raw MS/MS data were processed with Thermo Proteome Discoverer 2.5.0, and the MS/MS spectra were searched against the UniProt database of tryptic peptides from *Homo sapiens*, considering common contaminants. And other parameters were set as follows: 50 ppm precursor tolerance, fully tryptic peptides, fragment ion tolerance of 0.02 Da, and a static modification by TMT on lysine and peptide *N*-terminal. Carbamidomethylation of cysteine residues (+57.0214 Da) was set as a static modification, while oxidation of methionine residues (+15.9949 Da) and DBIA on cysteine residues (+239.1628) was set as variable modifications. Following protein identification, we performed bioinformatics analyses to annotate the identified proteins. Briefly, the UniProt database (version used: 2024_06) was our primary resource for retrieving functional information, including protein names, gene names, and known functions (more detailed experimental conditions can be found in Text S3). Moreover, to confirm the 6PPDQ-bonded mitochondrial proteins, the cell lysate (100 μg) from the 6PPDQ-exposure A549 cells (1.0×10^7) group was used for HPLC-ESI-Q-TOF-MS/MS analysis following the same procedures, but without TMTduplex labeling, and using iodoacetamide for alkylation of reduced cysteine residues instead of DBIA.

Mitochondrial Complex Activity Testing

Extraction buffer I of the mitochondrial respiratory chain complex activity detection kit [NADH-CoQ Reductase Activity Assay Kit and/or Cytochrome C Oxidase Activity Assay Kit (Solarbio, China)] was added to the cell pellet and homogenized 30 times in an ice bath. Sequential centrifugation steps were performed at 4 °C: first at 600 *g* for 10 min to collect the supernatant, followed by centrifugation of this supernatant at 11000 *g* for 15 min to obtain the mitochondrial pellet. After discarding the supernatant, the mitochondrial pellet was resuspended in a mixture of 200 μL of extraction buffer I and 200 μL of extraction buffer II of the detection kit. The suspension was sonicated using an ultrasonic disruptor (200 W power, 5 s sonication with 10 s intervals, repeated for 15 cycles) (Beyotime, China). The isolated mitochondria from A549 cells (1.0×10^7) that were treated respectively with DMSO (0.5%) and 6PPD (0.03 μM and 0.3 μM) as well as 6PPDQ (0.03 μM and 0.3 μM) were used to measure the mitochondrial electron transport chain complex activities. Complex I and Complex IV activities were determined on a SpectraMax iD3 (Molecular Devices, U.S.A.)

Measurement of Mitochondrial Membrane Potential ($\Delta\psi m$)

To determine the changes in mitochondrial membrane potential, JC-1 dye (Beyotime, China) was used. A549 cells (1.0×10^6) were cultured in a confocal culture dish (3.5 cm) for 24 h. After different treatments using DMSO (0.5%) and 6PPD (0.03 and 0.3 μM), as well as 6PPDQ (0.03 and 0.3 μM), cells were incubated with JC-1 for 20 min at 37 °C and then washed with JC-1 buffer solution 2 times. Confocal microscope images were obtained on a Leica SP8-STED 3X (Germany) using a 488 nm argon ion laser for excitation, monitoring the JC-1 monomer fluorescence at 530 nm, while using a 525 nm laser for excitation, monitoring JC-1 aggregates at 590 nm. The images were acquired with LAS X software in line-scanning mode with a resolution of 1024 × 1024 pixels and a scanning speed of 400 Hz. The relative fluorescence intensity was obtained using ImageJ software (https://imagej.net/).

https://doi.org/10.1021/acs.chemrestox.5c00250
Chem. Res. Toxicol. 2026, 39, 283−292

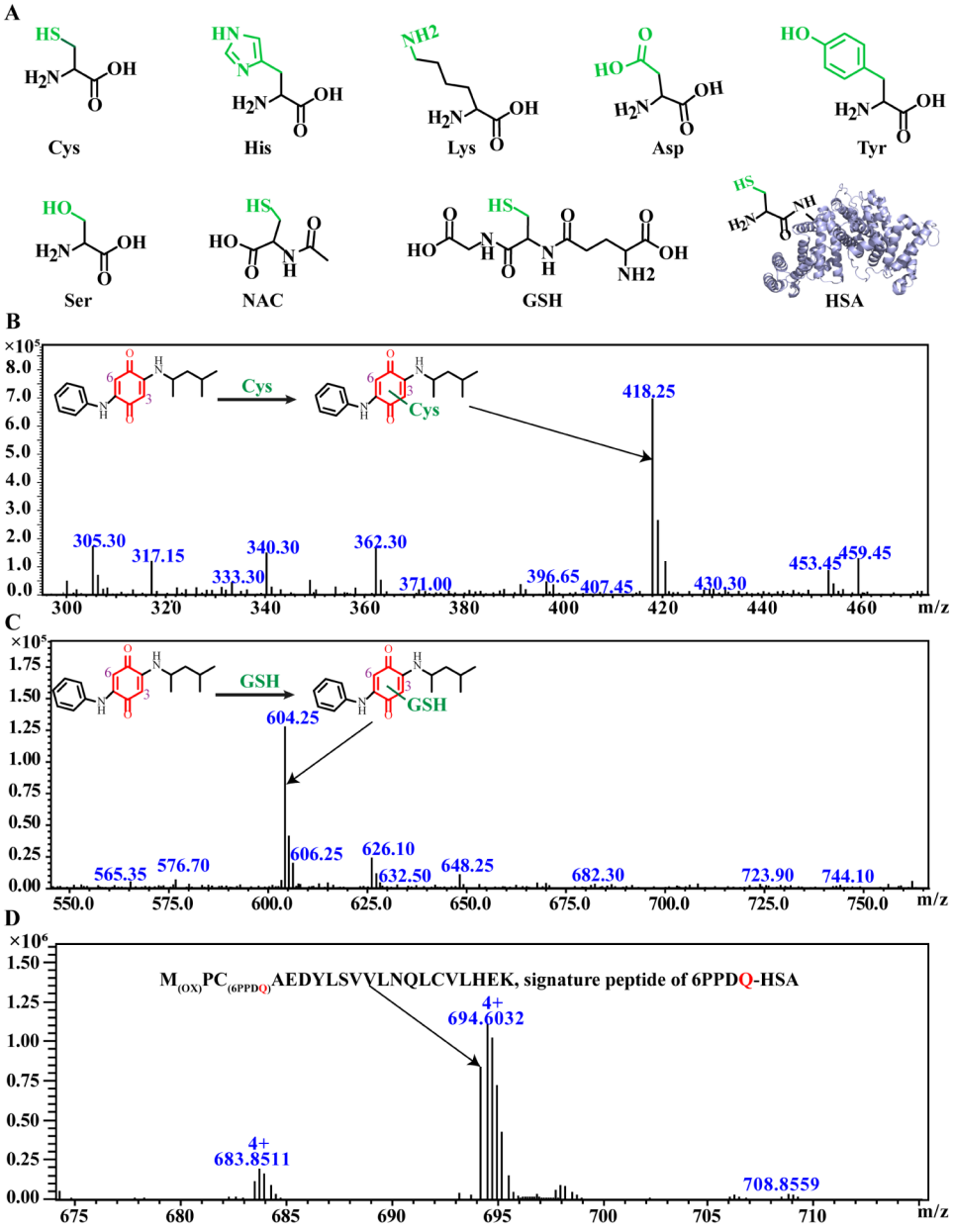

Figure 1. Nucleophilic compounds (A) tested for characterizing 6PPDQ reactivity, and the mass spectra of 6PPDQ-Cys (B), 6PPDQ-GSH (C), and 6PPDQ-signature peptide of HSA (D). Detailed experimental conditions can be found in the section of Experimental Methods.

Study of ROS Production in Mitochondria

ROS generation in mitochondria was detected using MitoSOX Red (MedChemExpress, China), a live-cell fluorescent probe that specifically targets mitochondria. A549 cells (1.0×10^6) were cultured in a confocal culture dish (3.5 cm) at 37 °C for 24 h under different treatments using DMSO (0.1%), 6PPD (0.03 and 0.3 μM), and 6PPDQ (0.03 and 0.3 μM), respectively. The cells were further incubated with 5 μM MitoSOX Red for 30 min in the dark and washed with PBS 3 times. Confocal microscope imaging was performed on a Leica SP8-STED 3X using a 488 nm argon ion laser and a HyD detector at 580 nm under a 63 × oil immersion objective.

Intracellular ATP Content Detection

After A549 cells were treated respectively with DMSO (0.5%) and 6PPD (0.03 and 0.3 μM), as well as 6PPDQ (0.03 and 0.3 μM) for 24 h, the cells were detached into centrifugation tubes and centrifuged at 12000 *g* for 5 min. An ATP Assay Kit (Acmec, China) was applied for the detection of the concentration of ATP in each group according to the manufacturer's instructions.

Density Functional Theory (DFT) Calculation

The theoretical calculations involved in this study were all performed using Gauss 09 D.01 and Multiwfn 3.8.[14,15] Geometrical optimization and vibrational frequencies of 6PPDQ were calculated using hybrid DFT at the B3LYP/def-SVP level, while nucleophilic amino acids were calculated using hybrid DFT at the B3LYP/6−31G(d) level. The condensed Fukui index of 6PPDQ was calculated at the B3LYP/def-TZVP level after geometrical optimization of its chemical structure, while those of the nucleophilic amino acids were calculated at the B3LYP/6−31G(d) level.

https://doi.org/10.1021/acs.chemrestox.5c00250
Chem. Res. Toxicol. 2026, 39, 283−292

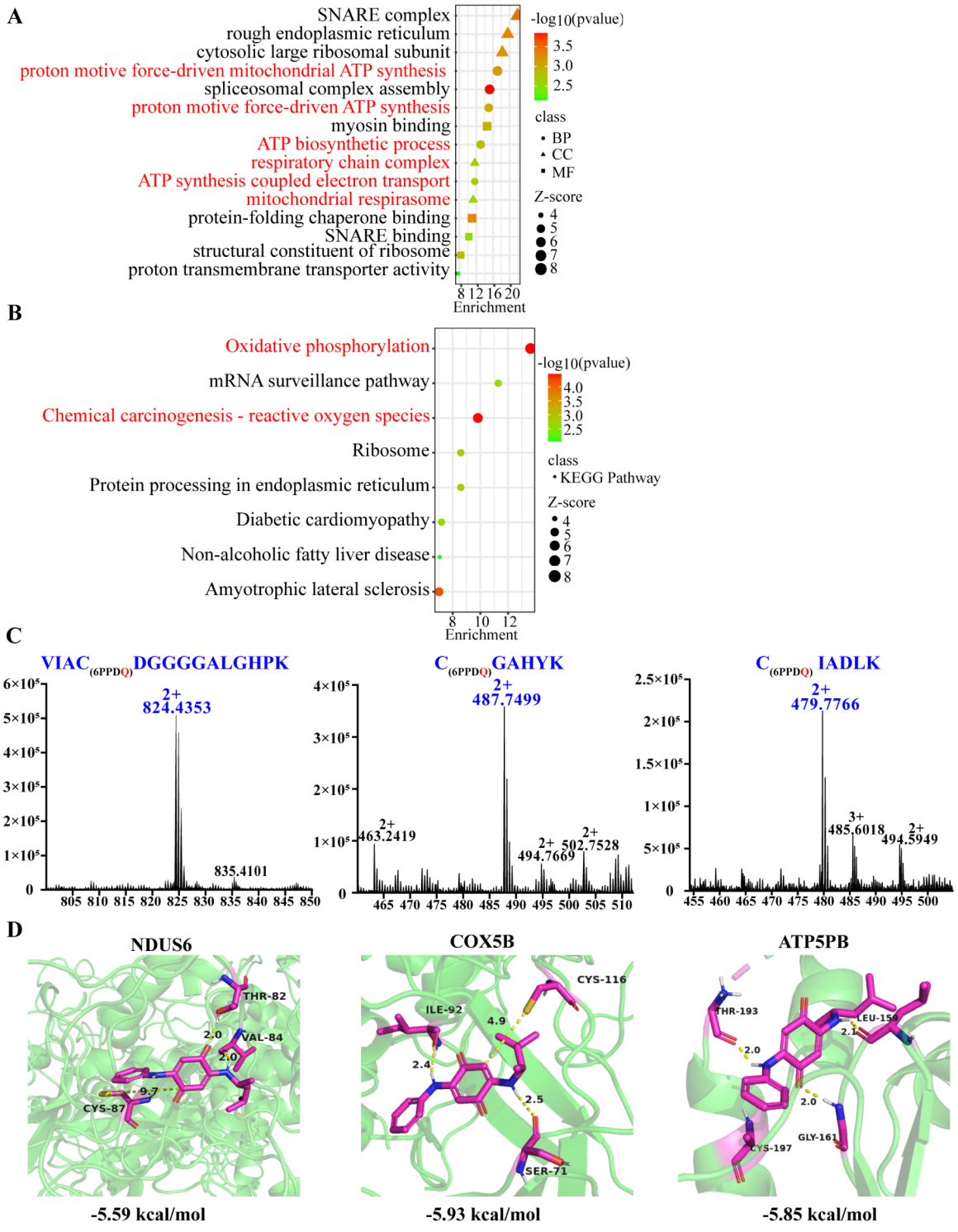

Figure 2. (A) GO enrichment analysis of the CR > 1.2 proteins was screened on the DBIA-based sulfhydryl-reactive proteomics platform (BP: biological process; CC: cellular component; MF: molecular function). The *p*-value measures the statistical significance of the enrichment result. A *p*-value less than 0.05 indicates that the enrichment is significant. The z-score represents the standard deviations by which the observed number of enriched genes and/or proteins deviates from the expected number under a random distribution. A larger absolute value of the z-score suggests a more significant enrichment. The enrichment score quantifies the degree to which a gene and/or protein set is overrepresented in a particular GO term or pathway. A higher enrichment score indicates greater enrichment. (B) KEGG pathway analysis of the CR > 1.2 proteins was screened on the DBIA-based sulfhydryl-reactive proteomics platform. (C) Mass spectra of 6PPDQ binding to the signature peptides of NDUS6, COX5B, and ATP5PB. (D) Docking analysis of 6PPDQ with NDUS6, COX5B, and ATP5PB.

GO and KEGG Analysis

Gene Ontology (GO) and Kyoto Encyclopedia of Genes and Genomes (KEGG) analysis were performed using the Metascape online web server (v3.5.20240901)[16] to assess the enrichment of the 6PPDQ-bonded proteins. The protein symbol of each candidate was used as the input data. The *p*-

https://doi.org/10.1021/acs.chemrestox.5c00250
Chem. Res. Toxicol. 2026, 39, 283−292

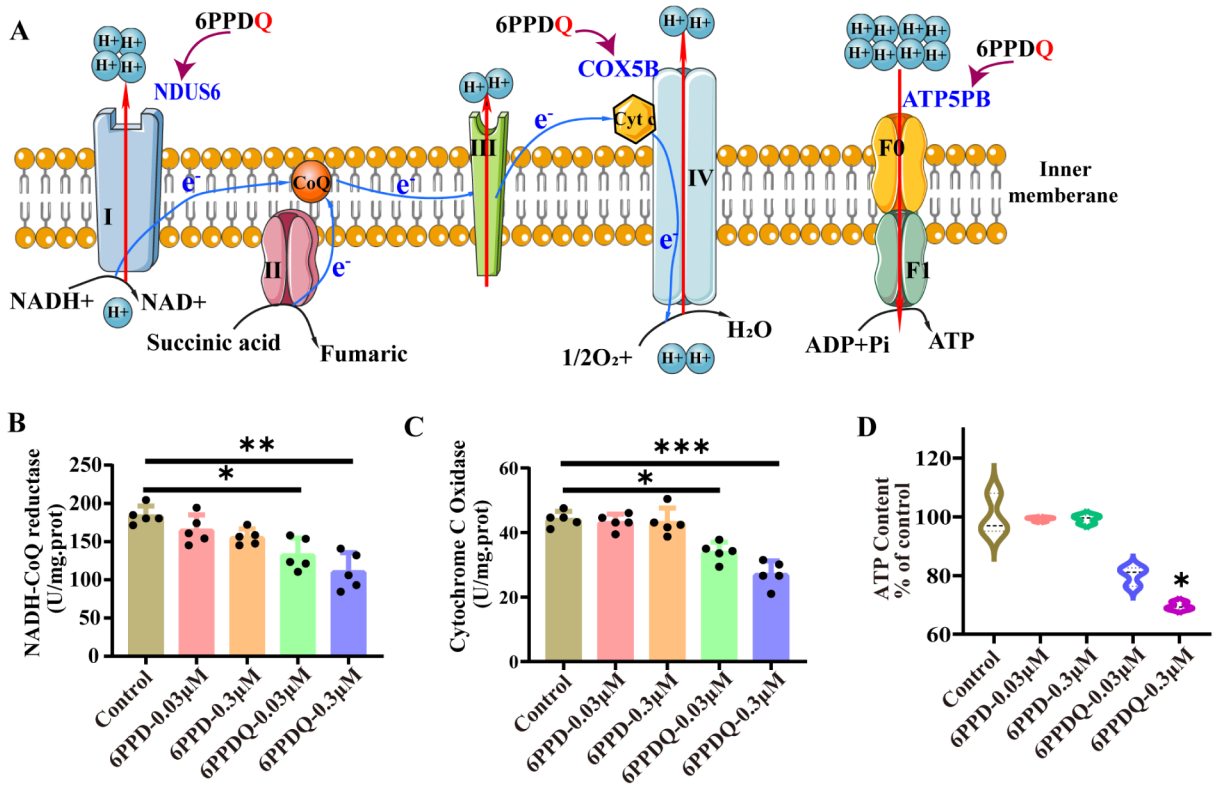

Figure 3. (A) 6PPDQ covalently binds to NDUS6, COX5B, and ATP5PB proteins, which are located on the inner mitochondrial membrane and serve as essential subunits of mitochondrial Complex I, Complex IV, and ATP synthase, respectively. Complex I initiates the mitochondrial respiratory chain, accepting electrons from the reduced nicotinamide adenine dinucleotide (NADH) and transferring them to coenzyme Q (ubiquinone). Simultaneously, Complex I pumps protons (H^+) from the mitochondrial matrix to the intermembrane space. Complex IV functions as the terminal enzyme of the mitochondrial respiratory chain, accepting electrons from cytochrome c and transferring them to oxygen (O_2) to ultimately form water. Concurrently, Complex IV also pumps protons into the intermembrane space. ATP synthase is the crucial enzyme in oxidative phosphorylation, utilizing the proton concentration gradient (proton motive force) across the inner mitochondrial membrane to phosphorylate adenosine diphosphate (ADP) to ATP. (B) The effects of 6PPD and 6PPDQ on the enzyme activity of mitochondrial oxidative respiratory chain Complex I (data are shown as mean ± SD, $n = 5$, * $p < 0.05$, ** $p < 0.01$, as compared to the control). (C) The effects of 6PPD and 6PPDQ on the enzyme activity of mitochondrial oxidative respiratory chain Complex IV (data are shown as mean ± SD, $n = 5$, * $p < 0.05$, *** $p < 0.005$, as compared to the control). (D) The ATP content alterations in A549 cells under the exposure of 6PPD and 6PPDQ (data are shown as mean ± SE, $n = 3$, * $p < 0.05$, as compared to the control).

values <0.01 suggest significantly enriched categories in the subontology of biological process, molecular function, cellular component, and KEGG pathway.

Docking Processing

The structures of NDUS6 (PDB ID: 5XTB), COX5B (PDB ID: 5Z62) and ATP5PB (PDB ID: 8H9 V) were obtained from the RCSB PDB database (https://www.rcsb.org/). The poses and vacuum electrostatic surfaces of 6PPDQ and the proteins were presented by Pymol (https://pymol.org/2/). The binding affinity analysis was processed by Autodock Tools 1.5.6.[17]

Statistical Analysis

All experiments in this study were independently performed 3 times or more. The final results were presented as the mean values ± standard error (SE), and the figures were processed by GraphPad Prism 8 (GraphPad Software, Inc., San Diego, CA, U.S.A.). The data were tested by one-way analysis of variance (ANOVA) with Dunnett's multiple comparison test. These data meet the assumptions of parameteric testing, including normality and homogeneity of variances, using the Shapiro-Wilk test and Levene's test. A statistically significant difference was considered when the p-value was less than 0.05.

RESULTS & DISCUSSION

Chemical Reactivity of 6PPDQ toward Nucleophilic Amino Acids as well as Sulfhydryl-Containing Molecules

The α-carbon atoms adjacent to the carbonyl group (C-3 and/or C-6) in the 6PPDQ molecular structure (Scheme 1A) have stronger electrophilicity[18] to attack nucleophiles. We first selected nucleophilic amino acids (AAs), such as cysteine, lysine, tyrosine, serine, aspartic acid, and histidine, in proteins (Figure 1A) to react with 6PPDQ. Using either 0.03 or 0.3 μM 6PPDQ, HPLC-ESI-Q-TOF-MS studies indicated that Michael addition products between 6PPDQ and cysteine were formed (Figure 1B and Figure S1), but no reaction products between 6PPDQ and other nucleophilic amino acids were detected (Figure S2). These observed phenomena can be explained by chemical computational results, which show that the sulfhydryl of cysteine has a much higher condensed local nucleophilicity index (0.997 e·eV), calculated using Gauss 09 D.01 and Multiwfn 3.8 software, than those of the ε-amino group of lysine (0.565), the phenolic hydroxyl of tyrosine (0.357), the hydroxyl of serine (0.228), the carboxyl of aspartic acid (0.146), and the imidazole of histidine (0.141) when they exist alone (Table S1). When 6PPDQ reacted with the N-terminal acetylation derivative of cysteine, N-acetyl cysteine

https://doi.org/10.1021/acs.chemrestox.5c00250
Chem. Res. Toxicol. 2026, 39, 283−292

(NAC), we found there are two Michael addition products with relative peak area 20.7% and 79.3% with identical m/z (460.20 Da) but different retention times (23.6 and 25.1 min) on HPLC-ESI-Q-TOF-MS (Figure S3), implying that the C-3 and C-6 in the quinone moiety of 6PPDQ have different electrophilic reactivity toward the sulfhydryl of NAC. This is supported by the condensed Fukui $f+$ index prediction, indicating that the electrophilicity of C-3 (0.031) is higher than that of C-6 (0.024). ^{1}H NMR measurements further confirmed that the major product is formed via Michael addition at C-3 (Figure S4). The results observed between 6PPDQ and the sulfhydryl-containing tripeptide GSH (Figure 1C) and protein HSA (Figure 1D) further evidenced the chemical reactivity of the quinone moiety of 6PPDQ toward the sulfhydryl, which is in agreement with previous studies on the reaction between electrophilic pollutants and thiols.[19] Subsequently, we further focused on the investigation of the interaction of 6PPDQ with the proteins in cells to find 6PPDQ-bonded proteins and understand the underlying molecular mechanism of 6PPDQ's toxicity.

Discovery of 6PPDQ-Bonded Mitochondrial Proteins in A549 Cells That Cause the Dysfunction of Mitochondria

Scheme 1B shows the sulfhydryl-reactive proteomics platform we established, on which the interactions of 6PPDQ directly with the proteins in A549 cells can be found. DBIA labeled all the reactive cysteine residues on the proteins in the control group, while it only labeled the cysteine residues of 6PPDQ-unreacted proteins in the 6PPDQ-exposure group. The ratio between the mass-to-charge signal intensities of the labeled TMT-126 and TMT-127 mass reporters was defined as the competition ratio (CR), reflecting the binding degree of 6PPDQ toward the protein targets in A549 cells. Based on the threshold of a CR value greater than 1.2, which implies significant involvement of the cysteine residue, we extracted 82 6PPDQ-bonded proteins from the 3,436 sulfhydryl-reactive proteins detected in A549 cells (Scheme 1C, Figure S5 and Table S2). GO enrichment analysis revealed that these 6PPDQ-bonded proteins predominantly distribute in the mitochondrial respiratory complexes, besides significantly enriching proton transmembrane transport and ATP synthesis-coupled electron transport processes, suggesting their central roles in cellular energy metabolism (Figure 2A). KEGG pathway analysis further suggested that these 6PPDQ-bonded proteins significantly enrich in the key pathways (Figure 2B), especially in oxidative phosphorylation, which is closely associated with chemically reactive oxygen species (ROS) pathways, implying that 6PPDQ might induce cellular damage by interfering with oxidative stress responses. Taken together, both GO and KEGG analyses suggested that 6PPDQ-bonded proteins could be involved in the regulation of oxidative phosphorylation in mitochondria-related biological processes. Along with these clues, we re-extracted the data obtained from the sulfhydryl-reactive proteomics platform, while performing the experiments without using DBIA and TMT labeling. We found three suspicious 6PPDQ-bonded proteins located on the inner mitochondrial membrane: NDUS6 (6PPDQ binds with Cys-87; CR = 1.48), COX5B (Cys-116; CR = 1.53), and ATP5PB (Cys-239; CR = 1.52) (Scheme 1C and Figure 2C). The molecular docking analysis supported the favorable binding of 6PPDQ to the cysteine residues located in the functional domains of these three proteins, with binding energies of −5.59, −5.93, and −5.86 kcal/mol (Figure 2D), respectively, which are much lower than that (−1.26 kcal/mol) of 6PPDQ with GSH (Figure S6).

These three 6PPDQ-bonded mitochondrial membrane proteins are the key components in mitochondrial respiratory chain electron transfer and ATP synthesis processes (Figure 3A). NDUS6, as an essential subunit of Complex I of the mitochondrial oxidative respiratory chain, participates in NADH dehydrogenase activity regulation.[20] Binding of 6PPDQ to the Cys-87 (Figure 2C and D) that is at a β-turn position of NDUS6 (https://www.ebi.ac.uk/pdbe/entry/pdb/5XTB) may disrupt intermolecular hydrogen bonds and thus the β-turn status, potentially altering the intrinsic configuration of NDUS6 and thus leading to Complex I assembly partially failure. This was evidenced by the results obtained from Complex I activity testing experiments using the NADH-CoQ Reductase Activity Assay Kit. The activity decreased by 27.63% ($p < 0.05$) under the exposure of 0.03 μM (8.94 μg/L) 6PPDQ and by 39.63% ($p < 0.01$) under 0.3 μM (89.4 μg/L) 6PPDQ compared to the control (Figure 3B). It should be noted that exposure of 6PPD with the same concentrations as those of 6PPDQ caused an insignificant reduction of 10.04% ($p = 0.2$) and 15.38% ($p = 0.08$) in the complex I activity (Figure 3B). COX5B is a core component of cytochrome C oxidase and Cys-116 of COX5B participates in Zn^{2+} coordination that stabilizes cytochrome a3 and copper B (CuB) in the mitochondrial Complex IV redox site.[21] Binding of 6PPDQ to Cys-116 (Figure 2C and D) may disturb its structural stabilization role of Zn^{2+}, possibly leading to changes in the overall assembly of complex IV and affecting its function. The Complex IV activity experiments using Cytochrome C Oxidase Activity Assay Kit indicated that its activity is attenuated at 23.11% ($p < 0.05$) and 38.63% ($p < 0.005$) under the exposure of 0.03 and 0.3 μM 6PPDQ relative to the control (Figure 3C), but 6PPD did not cause any significant decrease. ATP5PB is an important constituent of the ATP synthase F1F0 Complex, as an essential subunit of the F0 portion, playing a crucial role in mitochondrial oxidative phosphorylation. As a key subunit of the peripheral stalk of mitochondrial ATP synthase, ATP5PB plays a crucial role in maintaining the structural stability of the enzyme complex.[22] The binding of 6PPDQ to the Cys-239 residue of ATP5PB (Figure 2C and D) likely disrupts the interaction between ATP5PB and the OSCP subunit through steric hindrance or allosteric effects. The functional coupling between these two components is important for maintaining the mechanical stability of the F1 catalytic subunit of ATP synthase. When this interaction is perturbed, the rotational movement of the catalytic subunit is prone to abnormal torsional, damaging the ATP synthesis generation rate. Exposure, respectively, to 0.03 and 0.3 μM 6PPDQ resulted in decreases in ATP contents of 19.94% ($p = 0.07$) and 30.39% ($p < 0.05$) compared to the control (Figure 3D). Although these findings may be related to the potential inhibition of ATP5PB by 6PPDQ, it must be recognized that the ATP synthesis efficiency is also affected by the functional state of the entire respiratory chain. Therefore, the observed decrease in ATP levels may also partly result from the inhibition of respiratory chain Complex I and Complex IV activities, which would reduce the proton motive force needed to drive ATP synthase. Actually, we know that these proteins do not function independently but synergistically, like correlated units in a machine, for maintaining mitochondrial oxidative phosphorylation and cellular energy balance. Their functional deficiencies led to various mitochondrial dysfunc-

https://doi.org/10.1021/acs.chemrestox.5c00250
Chem. Res. Toxicol. 2026, 39, 283−292

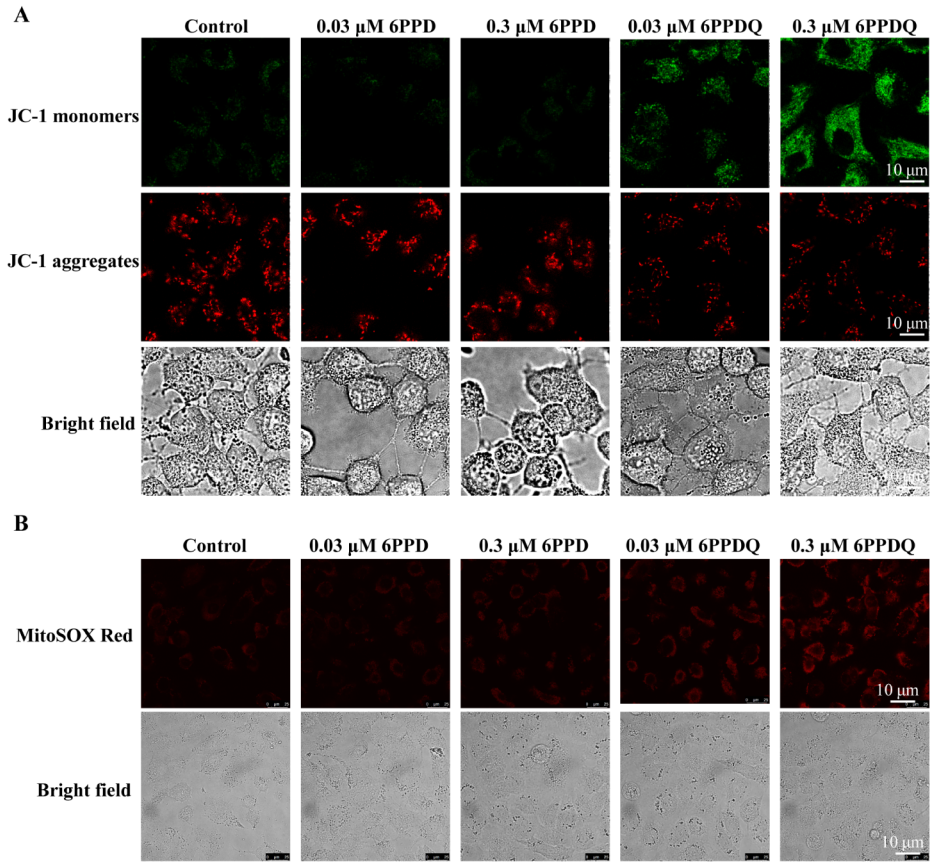

Figure 4. (A) Representative confocal imaging shows the mitochondrial membrane potential $\Delta\psi m$ alterations in A549 cells treated with DMSO (0.5%), 6PPD and 6PPDQ (0.03 and 0.3 μM). JC-1 monomers: $\lambda_{ex}/\lambda_{em}$ = 488 nm/530 nm; JC-1 aggregates: $\lambda_{ex}/\lambda_{em}$ = 525 nm/590 nm. (B) Representative confocal imaging shows the mitochondrial reactive oxygen species levels alterations in A549 cells treated with DMSO (0.5%), 6PPD and 6PPDQ (0.03 and 0.3 μM). MitoSOX Red: $\lambda_{ex}/\lambda_{em}$ = 488 nm/580 nm.

tion, as demonstrated by the phenomena we observed in confocal microscopy imaging using the JC-1 fluorescent probe (Figure 4A), i.e., a reduced mitochondrial membrane potential ($\Delta\psi m$) in A549 cells, as the green fluorescence signal of JC-1 monomers increased 3.2-fold and 6.7-fold under the exposure of 0.03 and 0.3 μM 6PPDQ compared to that of the control (Figure S7A). The mitochondrial ROS levels, 2.2-fold higher (0.03 μM 6PPDQ) and 3.8-fold higher (0.3 μM 6PPDQ), detected using the MitoSOX Red fluorescent probe compared to the control, were also observed (Figure 4B and Figure S7B). This phenomenon is reasonable[23−25] and can be explained by disruptions in electron transport chain (ETC) function responses. Inhibition of specific ETC complexes (e.g., Complexes I, III, or IV) can lead to electron accumulation at upstream sites, increasing the likelihood of electron leakage to oxygen, thereby generating superoxide radicals even under reduced $\Delta\psi m$ conditions.[26] The inhibitory effect of 6PPDQ on the mitochondrial oxidative phosphorylation system is primarily manifested as the inhibition of enzyme activities of Complexes I and IV, leading to impaired electron transport chain function. This inhibition may cause electron transfer barriers and increased electron leakage while reducing the efficiency of proton pumping from the mitochondrial matrix to the intermembrane space. This series of changes further results in increased production of ROS and decreased $\Delta\psi m$.

The mitochondrial dysfunction likely induced by the three conserved mitochondrial 6PPDQ-bonded proteins, formed via the reaction between the ubiquitous protein cysteine sulfhydryl and the quinone in 6PPDQ, may represent a possible molecular mechanism underlying 6PPDQ's toxic behavior. A previous study on 6PPDQ's toxicity in mammalian dopaminergic primary neurons indicated that 6PPDQ induced mitochondrial dysfunction, manifested as significantly elevated mitochondrial ROS levels and markedly reduced mitochondrial membrane potential $\Delta\psi m$.[6] A study on primary cultured gill cells of rainbow trout (*Oncorhynchus mykiss*), an aquatic organism model, observed an increased oxygen consumption rate by uncoupling the mitochondrial electron transport chain.[27] As well, the studies on the invertebrate model organism *Caenorhabditis elegans* pointed out that 6PPDQ exposure could lead to impaired functionality of mitochondrial respiratory chain Complexes I and II.[28] All of these reports support our findings. Therefore, the three 6PPDQ-bonded proteins discovered in the mitochondria may deserve to be key proteins to elucidate the cytotoxicity of 6PPDQ at the molecular level.

CONCLUSION

6PPDQ's electrophilic quinone moiety directly binding to the ubiquitous nucleophilic cysteine residue as an initiating molecular event lays the foundation for its potential broad-spectrum toxicity. The three 6PPDQ-bonded mitochondrial proteins, NDUS6, COX5B, and ATP5PB, discovered from the human model cell line A549 on the sulfhydryl-reactive proteomics platform, should be responsible for mitochondrial dysfunction. The three 6PPDQ-bonded proteins are highly

https://doi.org/10.1021/acs.chemrestox.5c00250
Chem. Res. Toxicol. 2026, 39, 283−292

conserved throughout evolution, and the mitochondrial oxidative phosphorylation process is involved universally as a core energy metabolism pathway in almost all aerobic organisms, implying the possibility of the broad-spectrum toxicity of 6PPDQ. Clearly, in-depth investigation should be further performed for a more comprehensive understanding of the cytotoxic features of 6PPDQ. While the interaction of the electrophilic quinone moiety in 6PPDQ with protein sulfhydryl groups appears to be responsible for its broad-spectrum toxicity as described above, the alkyl side chain in the 6PPDQ molecular structure[29,30] and the key protein functional domain where the reactive sulfhydryl is located are crucial for the acute species-specific toxicity of 6PPDQ toward 6PPDQ-sensitive biological models, such as coho salmon (*Oncorhynchus kisutch*), which need to be extensively and intensively investigated in the future.

■ ASSOCIATED CONTENT

Supporting Information

The Supporting Information is available free of charge at https://pubs.acs.org/doi/10.1021/acs.chemrestox.5c00250.

Methods; HPLC-ESI-Q-TOF-MS chromatograms of the products between 6PPDQ and cysteine (Figure S1); HPLC-ESI-Q-TOF-MS chromatograms of the products between 6PPDQ and nucleophilic amino acids (Figure S2); HPLC-ESI-Q-TOF-MS chromatograms of the products between 6PPDQ and NAC (Figure S3); ^{1}H NMR spectra of 6PPDQ and 6PPDQ-NAC (Figure S4); The proteins identified by the DBIA-mediated sulfhydryl-reactive proteomics platform and the distribution of their CR values (Figure S5); Docking analysis of 6PPDQ with GSH (Figure S6); The relative JC-1 monomer and MitoSOX Red intensities of 6PPD and 6PPDQ-exposure (0.03, 0.3 μM) groups compared with the control DMSO (0.5%) group (Figure S7); Condensed local nucleophilicity index of amino acids (Table S1); (Proteins with CR > 1.2 identified on the DBIA-mediated sulfhydryl-reactive proteomics platform (Table S2) (PDF)

■ AUTHOR INFORMATION

Corresponding Authors

Xiaowen Yan − *Department of Chemistry and the MOE Key Laboratory of Spectrochemical Analysis & Instrumentation, College of Chemistry and Chemical Engineering, Xiamen University, Xiamen 361005, China;* orcid.org/0000-0001-6608-6044; Email: xwyan@xmu.edu.cn

Qiuquan Wang − *Department of Chemistry and the MOE Key Laboratory of Spectrochemical Analysis & Instrumentation, College of Chemistry and Chemical Engineering, Xiamen University, Xiamen 361005, China;* orcid.org/0000-0002-5166-4048; Email: qqwang@xmu.edu.cn

Authors

Naijie Wei − *Department of Chemistry and the MOE Key Laboratory of Spectrochemical Analysis & Instrumentation, College of Chemistry and Chemical Engineering, Xiamen University, Xiamen 361005, China*

Mingyue Yu − *Department of Chemistry and the MOE Key Laboratory of Spectrochemical Analysis & Instrumentation, College of Chemistry and Chemical Engineering, Xiamen University, Xiamen 361005, China*

Rong Li − *Department of Chemistry and the MOE Key Laboratory of Spectrochemical Analysis & Instrumentation, College of Chemistry and Chemical Engineering, Xiamen University, Xiamen 361005, China*

Zhixin Xiao − *Department of Chemistry and the MOE Key Laboratory of Spectrochemical Analysis & Instrumentation, College of Chemistry and Chemical Engineering, Xiamen University, Xiamen 361005, China*

Shi Chen − *Department of Chemistry and the MOE Key Laboratory of Spectrochemical Analysis & Instrumentation, College of Chemistry and Chemical Engineering, Xiamen University, Xiamen 361005, China*

Limin Yang − *Department of Chemistry and the MOE Key Laboratory of Spectrochemical Analysis & Instrumentation, College of Chemistry and Chemical Engineering, Xiamen University, Xiamen 361005, China*

Qian Liu − *State Key Laboratory of Environmental Chemistry and Ecotoxicology, Research Center for Eco-Environmental Sciences, Chinese Academy of Sciences, Beijing 100085, China;* orcid.org/0000-0001-8525-7961

Guibin Jiang − *State Key Laboratory of Environmental Chemistry and Ecotoxicology, Research Center for Eco-Environmental Sciences, Chinese Academy of Sciences, Beijing 100085, China;* orcid.org/0000-0002-6335-3917

Complete contact information is available at: https://pubs.acs.org/10.1021/acs.chemrestox.5c00250

Notes

The authors declare no competing financial interest.

■ ACKNOWLEDGMENTS

This study was supported by the National Natural Science Foundation of China (No. 22193053, 22576171, 22193050, and 22074127).

■ REFERENCES

(1) Tian, Z.; Zhao, H.; Peter, K. T.; Gonzalez, M.; Wetzel, J.; Wu, C.; Hu, X.; Prat, J.; Mudrock, E.; Hettinger, R.; Cortina, A. E.; Biswas, R. G.; Kock, F. V. C.; Soong, R.; Jenne, A.; Du, B.; Hou, F.; He, H.; Lundeen, R.; Gilbreath, A.; Sutton, R.; Scholz, N. L.; Davis, J. W.; Dodd, M. C.; Simpson, A.; McIntyre, J. K.; Kolodziej, E. P. A ubiquitous tire rubber-derived chemical induces acute mortality in coho salmon. *Science* **2021**, *371* (6525), 185−189.

(2) Song, Z.; Yu, X.; Zhu, M.; Wu, Z.; Fu, Z.; Chen, J. Distinct Species-Specific and Toxigenic Metabolic Profiles for 6PPD and 6PPD Quinone by P450 Enzymes: Insights from In Vitro and In Silico Studies. *Environ. Sci. Technol.* **2024**, *58* (34), 14994−15004.

(3) Hua, X.; Wang, D. Tire-rubber related pollutant 6-PPD quinone: A review of its transformation, environmental distribution, bioavailability, and toxicity. *J. Hazard. Mater.* **2023**, *459*, 132265.

(4) Chen, X.; He, T.; Yang, X.; Gan, Y.; Qing, X.; Wang, J.; Huang, Y. Analysis, environmental occurrence, fate and potential toxicity of tire wear compounds 6PPD and 6PPD-quinone. *J. Hazard. Mater.* **2023**, *452*, 131245.

(5) Du, B.; Liang, B.; Li, Y.; Shen, M.; Liu, L.-Y.; Zeng, L. First Report on the Occurrence of N-(1,3-Dimethylbutyl)-N′-phenyl-p-phenylenediamine (6PPD) and 6PPD-Quinone as Pervasive Pollutants in Human Urine from South China. *Environ. Sci. Technol. Lett.* **2022**, *9* (12), 1056−1062.

(6) Fang, J.; Wang, X.; Cao, G.; Wang, F.; Ru, Y.; Wang, B.; Zhang, Y.; Zhang, D.; Yan, J.; Xu, J.; Ji, J.; Ji, F.; Zhou, Y.; Guo, L.; Li, M.; Liu, W.; Cai, X.; Cai, Z. 6PPD-quinone exposure induces neuronal mitochondrial dysfunction to exacerbate Lewy neurites formation induced by α-synuclein preformed fibrils seeding. *J. Hazard. Mater.* **2024**, *465*, 133312.

(7) Liu, C.; Zhao, X.; Guo, L.; Yu, Q.; Zhang, W.; Peng, Z.; Gao, Y.; Gong, X.; Li, P.; Jiao, H.; Zhou, T.; Zhang, Q.; Song, S.; Jiang, G. Emerging N-(1,3-dimethylbutyl)-N'-phenyl-p-phenylenediamine (6PPD) and 6PPD quinone in paired human plasma and urine from Tianjin, China: Preliminary assessment with demographic factors. *J. Hazard. Mater.* **2024**, *476*, 134818.
(8) Yang, Y.; Meng, W.; Zhang, Y.; Meng, W.; Li, J.; Liu, W.; Su, G. Characterizing the Metabolism of Tire Rubber-Derived p-Phenylenediamine Quinones to Identify Potential Exposure Biomarkers in Humans. *Environ. Sci. Technol.* **2024**, *58* (41), 18098−18108.
(9) Han, M.; Xia, K.; Xue, Y.; Yue, F.; Li, J.; Kang, F.; Zhu, B.; Hu, L.; Liu, Q.; Xie, Z.; Jiang, G. Emergence of More Potent PPD-Qs beyond 6PPD-Q in Human Blood and Cerebrospinal Fluid. *Environ. Sci. Technol. Lett.* **2025**, *12* (5), 496−502.
(10) Wan, X.; Liang, G.; Wang, D. Potential human health risk of the emerging environmental contaminant 6-PPD quinone. *Sci. Total Environ.* **2024**, *949*, 175057.
(11) Tian, L.; Zhao, S.; Zhang, R.; Lv, S.; Chen, D.; Li, J.; Jones, K. C.; Sweetman, A. J.; Peng, P. A.; Zhang, G. Tire Wear Chemicals in the Urban Atmosphere: Significant Contributions of Tire Wear Particles to PM2.5. *Environ. Sci. Technol.* **2024**, *58* (38), 16952−16961.
(12) Kuljanin, M.; Mitchell, D. C.; Schweppe, D. K.; Gikandi, A. S.; Nusinow, D. P.; Bulloch, N. J.; Vinogradova, E. V.; Wilson, D. L.; Kool, E. T.; Mancias, J. D.; Cravatt, B. F.; Gygi, S. P. Reimagining high-throughput profiling of reactive cysteines for cell-based screening of large electrophile libraries. *Nat. Biotechnol.* **2021**, *39* (5), 630−641.
(13) Li, J.; Van Vranken, J. G.; Pontano Vaites, L.; Schweppe, D. K.; Huttlin, E. L.; Etienne, C.; Nandhikonda, P.; Viner, R.; Robitaille, A. M.; Thompson, A. H.; Kuhn, K.; Pike, I.; Bomgarden, R. D.; Rogers, J. C.; Gygi, S. P.; Paulo, J. A. TMTpro reagents: a set of isobaric labeling mass tags enables simultaneous proteome-wide measurements across 16 samples. *Nat. Methods* **2020**, *17* (4), 399−404.
(14) Frisch, M. J.; Trucks, G. W.; Schlegel, H. B.; Scuseria, G. E.; Robb, M. A.; Cheeseman, J. R.; Scalmani, G.; Barone, V.; Petersson, G. A.; Nakatsuji, H., et al. *Gaussian 09, RevisionD.01*; Gaussian, Inc.: Wallingford CT, 2016.
(15) Lu, T.; Chen, F. Multiwfn: a multifunctional wavefunction analyzer. *J. Comput. Chem.* **2012**, *33* (5), 580−592.
(16) Zhou, Y.; Zhou, B.; Pache, L.; Chang, M.; Khodabakhshi, A. H.; Tanaseichuk, O.; Benner, C.; Chanda, S. K. Metascape provides a biologist-oriented resource for the analysis of systems-level datasets. *Nat. Commun.* **2019**, *10* (1), 1523.
(17) Morris, G. M.; Huey, R.; Lindstrom, W.; Sanner, M. F.; Belew, R. K.; Goodsell, D. S.; Olson, A. J. AutoDock4 and AutoDockTools4: Automated docking with selective receptor flexibility. *J. Comput. Chem.* **2009**, *30* (16), 2785−2791.
(18) Guo, X.; Mayr, H. Quantification of the Ambident Electrophilicities of Halogen-Substituted Quinones. *J. Am. Chem. Soc.* **2014**, *136* (32), 11499−11512.
(19) Suzuki, T.; Hidaka, T.; Kumagai, Y.; Yamamoto, M. Environmental pollutants and the immune response. *Nat. Immunol.* **2020**, *21* (12), 1486−1495.
(20) Wirth, C.; Brandt, U.; Hunte, C.; Zickermann, V. Structure and function of mitochondrial complex I. *Biochim. Biophys. Acta* **2016**, *1857* (7), 902−914.
(21) Comelli, R. N.; Viola, I. L.; Gonzalez, D. H. Characterization of promoter elements required for expression and induction by sucrose of the Arabidopsis COX5b-1 nuclear gene, encoding the zinc-binding subunit of cytochrome c oxidase. *Plant. Mol. Biol.* **2009**, *69* (6), 729−743.
(22) Yin, X.; Martinez, A. S.; Perkins, A.; Sparks, M. M.; Harder, A. M.; Willoughby, J. R.; Sepúlveda, M. S.; Christie, M. R. Incipient resistance to an effective pesticide results from genetic adaptation and the canalization of gene expression. *Evol. Appl.* **2021**, *14* (3), 847−859.
(23) Huo, X.; Wang, C.; Yu, Z.; Peng, Y.; Wang, S.; Feng, S.; Zhang, S.; Tian, X.; Sun, C.; Liu, K.; et al. Human transporters, PEPT1/2, facilitate melatonin transportation into mitochondria of cancer cells: An implication of the therapeutic potential. *J. Pineal. Res.* **2017**, *62* (4), No. e12390.
(24) Zhang, J.; Song, W.; Guo, J.; Zhang, J.; Sun, Z.; Ding, F.; Gao, M. Toxic effect of different ZnO particles on mouse alveolar macrophages. *J. Hazard. Mater.* **2012**, *219*−*220*, 148−155.
(25) Jiang, H.-Y.; Yang, Y.; Zhang, Y.-Y.; Xie, Z.; Zhao, X.-Y.; Sun, Y.; Kong, W.-J. The dual role of poly (ADP-ribose) polymerase-1 in modulating parthanatos and autophagy under oxidative stress in rat cochlear marginal cells of the stria vascularis. *Redox. Biol.* **2018**, *14*, 361−370.
(26) Makrecka-Kuka, M.; Dimitrijevs, P.; Domracheva, I.; Jaudzems, K.; Dambrova, M.; Arsenyan, P. Fused isoselenazolium salts suppress breast cancer cell growth by dramatic increase in pyruvate-dependent mitochondrial ROS production. *Sci. Rep.* **2020**, *10* (1), 21595.
(27) Mahoney, H.; da Silva Junior, F. C.; Roberts, C.; Schultz, M.; Ji, X.; Alcaraz, A. J.; Montgomery, D.; Selinger, S.; Challis, J. K.; Giesy, J. P.; Weber, L.; Janz, D.; Wiseman, S.; Hecker, M.; Brinkmann, M. Exposure to the Tire Rubber-Derived Contaminant 6PPD-Quinone Causes Mitochondrial Dysfunction In Vitro. *Environ. Sci. Technol. Lett.* **2022**, *9* (9), 765−771.
(28) Hua, X.; Liang, G.; Chao, J.; Wang, D. Exposure to 6-PPD quinone causes damage on mitochondrial complex I/II associated with lifespan reduction in Caenorhabditis elegans. *J. Hazard. Mater.* **2024**, *472*, 134598.
(29) Nair, P.; Barrett, H.; Tanoto, K.; Xie, L.; Sun, J.; Yang, D.; Yao, H.; Song, D.; Peng, H. Structure and Toxicity Characterization of Alkyl Hydroxylated Metabolites of 6PPD-Q. *Environ. Sci. Technol.* **2025**, *59* (15), 7474−7484.
(30) Nair, P.; Sun, J.; Xie, L.; Kennedy, L.; Kozakiewicz, D.; Kleywegt, S. M.; Hao, C.; Byun, H.; Barrett, H.; Baker, J.; Monaghan, J.; Krogh, E. T.; Song, D.; Peng, H. Synthesis and Toxicity Evaluation of p-Phenylenediamine-Quinones. *Environ. Sci. Technol.* **2025**, *59* (15), 7485−7494.

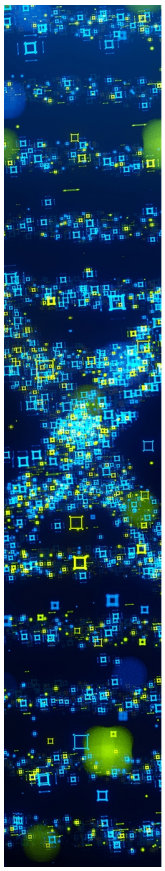
CAS BIOFINDER DISCOVERY PLATFORM™
STOP DIGGING THROUGH DATA —START MAKING DISCOVERIES
CAS BioFinder helps you find the right biological insights in seconds
Start your search
CAS
A division of the American Chemical Society

https://doi.org/10.1021/acs.chemrestox.5c00250
Chem. Res. Toxicol. 2026, 39, 283−292